Molecular Cancer Therapeutics

Vessel-Targeted Chemophototherapy with Cationic Porphyrin-Phospholipid Liposomes

Dandan Luo[1], Jumin Geng[1], Nasi Li[2], Kevin A. Carter[1], Shuai Shao[1], G. Ekin Atilla-Gokcumen[2], and Jonathan F. Lovell[1]

Abstract

Cationic liposomes have been used for targeted drug delivery to tumor blood vessels, via mechanisms that are not fully elucidated. Doxorubicin (Dox)-loaded liposomes were prepared that incorporate a cationic lipid; 1,2-dioleoyl-3-trimethylammonium-propane (DOTAP), along with a small amount of porphyrin-phospholipid (PoP). Near-infrared (NIR) light caused release of entrapped Dox via PoP-mediated DOTAP photo-oxidation. The formulation was optimized to enable extremely rapid NIR light-triggered Dox release (i.e., in 15 seconds), while retaining reasonable serum stability. *In vitro*, cationic PoP liposomes readily bound to both MIA PaCa-2 human pancreatic cancer cells and human vascular endothelial cells. When administered intravenously, cationic PoP liposomes were cleared from circulation within minutes, with most accumulation in the liver and spleen. Fluorescence imaging revealed that some cationic PoP liposomes also localized at the tumor blood vessels. Compared with analogous neutral liposomes, strong tumor photoablation was induced with a single treatment of cationic PoP liposomes and laser irradiation (5 mg/kg Dox and 100 J/cm^2 NIR light). Unexpectedly, empty cationic PoP liposomes (lacking Dox) induced equally potent antitumor phototherapeutic effects as the drug loaded ones. A more balanced chemo- and phototherapeutic response was subsequently achieved when antitumor studies were repeated using higher drug dosing (7 mg/kg Dox) and a low fluence phototreatment (20 J/cm^2 NIR light). These results demonstrate the feasibility of vessel-targeted chemophototherapy using cationic PoP liposomes and also illustrate synergistic considerations. *Mol Cancer Ther; 16(11); 2452–61. ©2017 AACR.*

Introduction

Tumor angiogenesis is requisite for tumor growth and metastasis (1–4). Therefore, one interesting anticancer strategy involves molecular targeting of therapeutics to tumor vasculature (5). This delivery approach has the advantage that tumor endothelial cells are freely accessible from blood, as opposed to the cancer and stromal cells inside tumors. Furthermore, high interstitial tumor fluid pressure creates less than ideal conditions to deliver therapeutics, which must extravasate from blood vessels (6). Endogenous tumor endothelial proteins have been identified for neovascular targeting including integrins (7), VEGFR (8), and CD105 (9). The RGD tripeptide, which binds to the $\alpha_v\beta_3$ integrin, was one of the earliest neovasculature targeting ligands used for drug delivery (doxorubicin), initially with drug–peptide conjugates (10) and targeted nanoparticles (11). Subsequently, targeted nanomaterials that can deliver cargo payloads to tumor vasculature have been extensively explored (12).

Numerous independent studies have demonstrated that cationic liposomes target tumor endothelial cells (13–19). The mechanism is not clear, but is likely due to differential neovascular expression of surface receptors and negatively charged macromolecules such as glycoproteins, anionic phospholipids, and proteoglycans (19, 20). Cationic liposomes that incorporate paclitaxel (EndoTag) are undergoing clinical trials in pancreatic cancer (21).

Photodynamic therapy (PDT) is an ablative technique that has been used for various indications, including to treat solid tumors (22, 23). Activatable and targeted PDT have been explored in numerous approaches (24–26). In the context of PDT, the term "vascular targeting" usually refers to application of the phototreatment while administered photosensitizers have high blood concentration, resulting in vascular damage (27, 28). However, there have also been numerous preclinical research studies involving actual molecular targeting of nanoparticulate photosensitizers to tumor endothelium for PDT (12, 29–31).

Our group recently developed porphyrin-phospholipid (PoP) liposomes that can be permeabilized by near-infrared (NIR) light and release encapsulated contents (32). Various anticancer agents such as doxorubicin (33, 34), irinotecan (35), and mitoxantrone (36) have been encapsulated into PoP liposomes for antitumor phototreatments in human pancreatic cancer xenografts in mice. Chemophototherapy (CPT), the combination of chemotherapy and phototherapy, is emerging as a potent ablation modality for solid tumors (37–41). PoP liposomes are well-suited for CPT because they represent a single agent and are capable of robust light-induced drug release. Besides enabling the light triggering release functionality of the liposomes, PoP also serves as a PDT agent itself. 1,2-Dioleoyl-3-trimethylammonium-propane (DOTAP) is a positively charged lipid used in many cationic liposome formulations (including clinical ones). In this work, DOTAP is incorporated into PoP liposomes for vessel-targeted CPT.

[1]Department of Biomedical Engineering, University at Buffalo, State University of New York, Buffalo, New York. [2]Department of Chemistry, University at Buffalo, State University of New York, Buffalo, New York.

Note: Supplementary data for this article are available at Molecular Cancer Therapeutics Online (http://mct.aacrjournals.org/).

Corresponding Author: Jonathan F. Lovell, University at Buffalo, State University of New York, 210 Bonner Hall, Buffalo 14260. Phone: 716-645-1020; Fax: 716-645-1020; E-mail: jflovell@buffalo.edu

doi: 10.1158/1535-7163.MCT-17-0276

Materials and Methods

Liposome preparation

The following lipids were obtained from Corden Pharma: 1,2-distearoyl-sn-glycero-3-phosphocholine (DSPC; # LP-R4-076), cholesterol (# CH-0355), 1,2-dioleoyl-sn-glycero-3-phosphocholine (DOPC; # LP-R4-070), and DOTAP (# LP-R4-117). The PoP used was sn-1-palmitoyl, sn-2-pyropheophorbide phosphtatidylcholine and was synthesized as previously reported (32). Various formulations were prepared by hot ethanol injection followed by pressurized extrusion as previously described (34, 42). The finalized cationic PoP liposome formulation was [DSPC:DOTAP:Cholesterol:PoP], [38:20:40:2] (mol%) at a drug to lipid molar ratio of 1:8. For other formulations, DOTAP was substituted for DSPC as indicated. To generate 5 mL PoP liposomes (20 mg/mL total lipids) of the indicated formulations, lipids were first fully dissolved in 1 mL of hot ethanol, followed by direct injection into 4 mL 250 mmol/L ammonium sulfate (pH 5.5) buffer at 60°C. The liposome solution was mixed and then passed 10 times at 60°C through sequentially stacked polycarbonate membranes of 0.2-, 0.1-, and 0.08-μm pore size using a 10 mL LIPEX nitrogen pressurized extruder (Northern Lipids). Free ammonium sulfate was removed by dialysis with buffer containing 10% sucrose and 10 mmol/L HEPES, pH = 7.8.

Dox loading and liposome characterization

Doxorubicin (LC Labs #D-4000) was actively encapsulated into the liposomes via ammonium sulfate gradient (43). A 20 mg/mL Dox solution was added to the liposomes at a drug to lipid molar ratio of 1:8 and incubated at 60°C for 1 hour. Liposome sizes and polydispersity were determined by dynamic light scattering via a NanoBrook 90 Plus PALS instrument in phosphate buffered saline (PBS). Zeta potential was measured by ZetaSizer in 10 mmol/L NaCI. Dox-loading efficacy was determined by a spin column filtration method. Liposomes were diluted in 25 mmol/L NaCl, and placed in a 100 kDa cutoff spin column (Pall, # OD100C34) and centrifuged at 2000 × *g* for 10 minutes. Unloaded Dox passed through the filter and was determined by UV spectroscopy. The loading efficacy was determined by a standard curve. Serum stability was assessed by incubating PoP liposomes (20 mg/mL lipids) diluted 200 times in 50% sterile bovine serum (Pel-Freeze # 37225) at 37°C for 1 hour. Triton X-100 (0.25%) was added, and Dox fluorescence was read. Dox release was calculated according to the formula: % Dox release = $(F_{Final} - F_{initial})/(F_{TX\text{-}100} - F_{initial}) \times 100\%$, where $F_{TX\text{-}100}$ is the fluorescence value when the liposomes are lysed with 0.25% Triton X-100 (Sigma, # X100-500ML).

Light-triggered drug release

Light-triggered release was performed with a power-tunable 665-nm laser diode (RPMC Lasers, LDX-3115-665) at the indicated fluence rates. Dox fluorescence was recorded in real time during irradiation in a fluorometer (PTI). Before laser irradiation at 250 mW/cm^2, 20 mg/mL PoP liposomes were diluted 400 times in 50% bovine serum and placed in a cuvette at 37°C. Temperature was measured by inserting a thermocouple probe (Atkins, # 39658-K) directly into the irradiated solution. Triton X-100 (0.25%) was added after laser irradiation to read the final fluorescence. Dox release was assessed by calculating Dox fluorescence before and after laser with the same formula above. Inhibition of Dox release by sodium sulfite or sodium ascorbate was performed in a cuvette with cationic 20 mg/mL PoP liposomes diluted 400 times in PBS containing 25 mmol/L sodium sulfite (J.T. Baker # 3922-01) or sodium ascorbate (VWR # 97061-072). Singlet oxygen sensor green (SOSG; Life Technologies # S-36002) was used for the detection of singlet oxygen generated by PoP during irradiation. SOSG fluorescence (exc./em. 504 nm/525 nm) was recorded during irradiation in a fluorometer. Light irradiation was performed in PBS containing SOSG.

Liquid chromatography–mass spectrometry (LC-MS)

Dox-loaded cationic PoP liposomes (20 mg/mL lipids) were diluted 100 times in PBS and irradiated (250 mW/cm^2) for 2 minutes. For oxidation inhibition study, samples were irradiated in PBS containing 25 mmol/L sodium sulfite. One mL of each liposome sample was then extracted with methanol:chloroform 1:2 (v/v) solution as previously described (42). The extracted lipids were then dried under vacuum and stored at −80°C before analysis. LC-MS data acquisition was performed using LC-ESI-QTOF (Agilent 1260 HPLC coupled to Agilent 6530 Accurate-Mass Quadrupole Time-of-Flight) in positive electrospray ionization mode. Chromatographic separation was achieved using a Luna C5 reversed phase column (5 μm, 4.6 mm × 50 mm, Phenomenex) with a C5 reversed-phase guard cartridge. Mobile phases A and B were 95:5 water:methanol (v/v) and 60:35:5 isopropanol:methanol:water, respectively. Each mobile phase was supplemented with 0.1% (v/v) formic acid and 5 mmol/L ammonium formate. The gradient started after 3 minutes at 0% B and then increased to 100% B over 10 minutes followed by 100% B for 7 minutes before equilibration for 8 minutes at 0% B. The flow rate was 0.5 mL/min. A JSI fitted electrospray ionization source was used. Capillary and fragmentor voltages were set to 3,500 and 175 V. Drying gas temperature was 350°C with a flow rate of 12 L/min. Data were collected using an m/z range of 50 to 1,700 in extended dynamic range.

For targeted analysis, the corresponding m/z for each ion was extracted in MassHunter Qualitative Analysis (version B.06.00, Agilent Technologies). Peak areas for each ion in extracted ion chromatogram were manually integrated and were presented as ion counts. Different collision energies were used to get optimal ionization. Fragmentation patterns were observed at 15, 35, and 55 V. In order to identify emerging species after irradiation, raw data obtained were imported into MassHunter Profinder (version B.06.00, Agilent Technologies) for peak alignment. Statistical analysis and filtering of the newly identified species were carried out in Mass Profinder Professional (version 12.6.1, Agilent Technologies).

In vitro studies

MIA PaCa-2 cells (ATCC # CRL-1420) or HUVECs (Promocell) were obtained originally in 2014, and frozen stocks were used without additional authentication. For confocal microscopy, 10,000 MIA PaCa-2 or HUVECs were seeded in eight-well confocal chamber slides (VWR # 43300-774) in DMEM media with 10% serum or endothelial cell growth medium (Cell Applications # 211-500). Twenty-four hours later, cells were incubated with 10 μg/mL Dox-loaded cationic PoP liposomes containing 5% or 20% DOTAP for 20 minutes. Media were replaced, and cells were washed before confocal imaging using a Zeiss LSM 710 confocal microscope at 20× objective. For quantification of cellular uptake of Dox and PoP, 10,000 MIA Paca-2 cells and HUVECs were seeded in 96-well plate in DMEM media with 10% serum or

endothelial cell growth medium, respectively. Twenty-four hours later, cells were incubated with 10 μg/mL Dox loaded in indicated PoP liposomes for 20 minutes. Cells were washed with PBS and lysed with 0.25% Triton X-100. Dox and PoP fluorescence signals were measured directly in a TECAN fluorescence plate reader. The percentage of cellular uptake of Dox and PoP was calculated by the fluorescence signal in the cells divided by the total amount of Dox or PoP added in the medium.

For fluorescence microscopy of tumor slices, tumor-bearing female nude mice were administered with 10 mg/kg Dox-loaded cationic PoP liposomes. Twenty-four hours later, 20 mg/kg Hoechst 33342 was injected 1 minute before sacrificing the mice to visualize the functional tumor vasculature. Tumors were removed and fixed in 10% formalin overnight followed by immersion in a 30% sucrose solution. Tissues were then embedded in OCT compound (VWR # 25608-930) in embedding molds, snap frozen in liquid nitrogen and stored at −80°C prior to use. Tumors were sectioned in a cryostat at −20°C at 10 μm thickness. Tumor slices were imaged with a Zeiss LSM 710 confocal microscope at 20 × objective.

Pharmacokinetics and biodistribution

Animal studies were carried out in accord with the University at Buffalo IACUC protocols. Female CD-1 mice (18–20 g, Charles River Laboratories) were intravenously injected via tail vein with Dox-loaded DOTAP/PoP liposomes or neutral DOPC liposomes at 10 mg/kg. Small blood volumes were sampled at 15 minutes, 1, 3, 6, 10, and 24 hours post injection for the DOPC liposome group and 15 minutes, 1 and 3 hours for the DOTAP/PoP liposome group. Blood was collected in a serum collection capillary tube (Microvette CB 300Z), and serum was obtained following centrifuged at 1,500 × *g* for 15 minutes. Serum was diluted in extraction buffer (0.075 N HCL, 90% isopropanol). Samples were then incubated at −20°C overnight and then centrifuged for 15 minutes at 10,000 × *g*. Supernatants were collected and analyzed by fluorescence in a 96-well plate reader, and Dox and PoP concentrations were determined by a standard curve. Noncompartmental pharmacokinetics parameters were analyzed by PKsolver.

For biodistribution studies, female nude mice (Jackson Labs, #007850) were inoculated with 5×10^6 MIA PaCa-2 cells. When tumor sizes reached 8 to 10 mm, mice were intravenously injected with 10 mg/kg Dox-loaded DOTAP/PoP liposomes and sacrificed 24 hours post injection. Tumors and key organs were collected and washed in PBS. Tissues (∼100 mg) were weighed and homogenized in 450 mL nuclear lysis buffer [250 mmol/L sucrose, 5 mmol/L Tris-HCl, 1 mmol/L $MgSO_4$, 1 mmol/L $CaCl_2$ (pH 7.6)] with a Bullet Blender Storm homogenizer. Homogenates (100 μL) were extracted with 900 μL 0.075 N HCI 90% isopropanol by mixing the samples and storage at −20°C overnight. Samples was removed and centrifuged at 10,000 × *g* for 15 minutes. The supernatant was collected, and the concentrations of Dox and PoP were determined fluorometrically.

Tumor growth inhibition

Five-week-old female nude mice (Jackson Labs, #007805) were inoculated with 5×10^6 Mia Paca-2 cells. When tumor sizes reached 5 to 8 mm (initial tumor volumes 70–120 mm^3), mice were randomly grouped into 5 groups, with 5 to 6 mice per group: (i) DOTAP/PoP liposomes + laser; (ii) DOPC Liposomes + laser; (iii) Empty DOTAP/PoP liposomes + laser; (iv) DOTAP/PoP liposomes − laser; (v) Saline. Dox-loaded DOTAP/PoP liposomes (200 μL; 5 mg/kg Dox, 1.4 mg/kg PoP) or empty DOTAP/PoP liposomes (1.4 mg/kg PoP) were intravenously injected via tail vein. Laser irradiation was initiated 15 minutes post injection for 8.3 minutes at 200 mW/cm^2 (665 nm, 100 J/cm^2) while mice were anesthetized. Tumor volumes were calculated using the ellipsoid formula: Volume $= \pi * L * \frac{W^2}{6}$, where L and W are the length and width of the tumor, respectively. Body weights of the mice were monitored for 4 weeks. Mice were sacrificed when tumor volumes exceeded 10 times the initial volumes or at the end of the study period (30 days).

For the second tumor growth inhibition study, mice were grouped as follows: (i) DOTAP/PoP liposomes + laser; (ii) Empty DOTAP/PoP liposomes + laser; (iii) DOTAP/PoP liposomes − laser; (iv) Saline. Dox-loaded DOTAP/PoP liposomes (7 mg/kg; 1.96 mg/kg PoP) or empty DOTAP/PoP liposomes (1.96 mg/kg PoP) were intravenously administrated. Mice were treated with 100 mW/cm^2 for 3 minutes 20 seconds (20 J/cm^2). Blood flow during this treatment was monitored using laser Doppler (moorLDI2-IR) in single spot mode. Before laser treatment, blood flow rate was stabilized for 10 minutes. After laser treatment was ended, tumor blood flow was monitored for another 100 seconds. During this period, mice were anesthetized and placed on a heating pad to maintain body temperature around 35°C. Tumor sizes were recorded 2 to 3 times per week by measuring tumor dimensions. Tumor volumes and body weight were measured according to the method above. Mice were sacrificed when tumor volumes exceeded 10 times of the initial volume or at the end of the study period (45 days).

Results

DOTAP accelerates light-triggered Dox release from PoP liposomes

DOTAP was titrated (in place of DSPC) into Dox-loaded liposomes comprising 0.5 mol% PoP, 40 mol% Cholesterol, and 59.5% mol DSPC. Increasing amount of DOTAP dramatically accelerated NIR light-triggered Dox release (Fig. 1A). Liposomes containing 10 and 20 mol% DOTAP were indistinguishable in terms of extremely rapid release, with 90% Dox release within 20 seconds. The time to reach 50% Dox release with varying DOTAP concentrations is shown in Fig. 1B. We recently demonstrated that unsaturated lipids such as DOPC can significantly enhance the light triggered release rate due to PoP-dependent unsaturated lipid photo-oxidation (42). Because DOTAP is also an unsaturated lipid and structurally similar to DOPC, we hypothesized that the mechanism of enhanced light-triggered release was related to oxidation of DOTAP. To assess whether DOTAP is oxidized following laser irradiation, LC-MS was used to quantify the presence of DOTAP before and after laser treatment. As shown in Fig. 1C, 97.5% of DOTAP was depleted after 665 nm laser treatment for 2 minutes at 250 mW/cm^2. New species were identified, including a species with m/z 726.5884 (Fig. 1D) and 694.5958, which are molecular weights that match oxidized DOTAP. The exact structures of the oxidized DOTAP were not determined; however, it is likely that both side chains of DOTAP were oxidized, forming a mixture of 9- and 10-hydroperoxides, as the species m/z 726.5884 matches the theoretical m/z (726.5878) of the product of this reaction. Illustrative peroxidized DOTAP structures with the correctly matching molecular weights are shown in Supplementary Fig. S1. When 25 mmol/L sodium sulfite

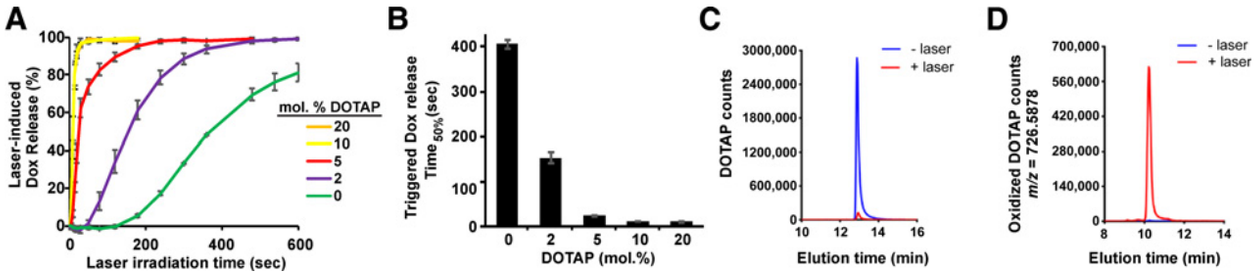

Figure 1.

DOTAP inclusion accelerates light-triggered Dox release in PoP liposomes. **A,** Light-triggered release of Dox from PoP liposomes (0.5 mol% PoP) containing indicated amount of DOTAP. Assessed in 50% bovine serum at 37°C under 250 mW/cm^2 irradiation from a 665 nm laser diode. **B,** Time required to reach 50% release Dox for PoP liposomes (0.5 mol% PoP) prepared with variable amount of DOTAP. **C,** DOTAP counts of PoP liposomes before and after irradiation for 2 minutes at 250 mW/cm^2. **D,** Counts for new lipid species corresponding to oxidized DOTAP generated after irradiation (m/z: 726.5878). Mean ± SD for $n = 4$.

was added to the liposome solution, it was found that the light-induced release of Dox was significantly inhibited (Supplementary Fig. S2A). When the antioxidant sodium ascorbate was added to the liposome solution, the release of Dox slowed but not as efficiently as sodium sulfite. With the presence of sodium sulfite, 84% of the DOTAP was protected from photo-oxidization (Supplementary Fig. S2B), further suggesting that PoP-dependent DOTAP photo-oxidization is responsible for membrane destabilization and drug release.

Characterization of cationic PoP liposomes

We previously demonstrated that the amount of PoP in the formulation will also affect the light-triggered cargo release rate (34, 42). By using SOSG, the amount of singlet oxygen generated was determined with liposomes containing various amounts of PoP. Figure 2A demonstrates that 2 mol% PoP generated the highest amount of singlet oxygen, as beyond that, self-quenching phenomenon likely started to occur. Thus, 2 mol% PoP was selected as the amount of PoP in the formulation. However, with 2 mol% PoP in the liposome, the Dox encapsulation efficacy was not ideal (below 90%) in formulations incorporating less than 5 mol% DOTAP (Fig. 2B). With PoP at 0.5 mol. %, DOTAP was not required to maintain robust loading efficacy. The zeta potential of PoP liposomes with 5, 10, 20, and 30 mol% DOTAP was determined to be 27.1, 33.9, 47.9, and 47.3 mV, respectively (Fig. 2C). The surface charge increased with increasing amount of

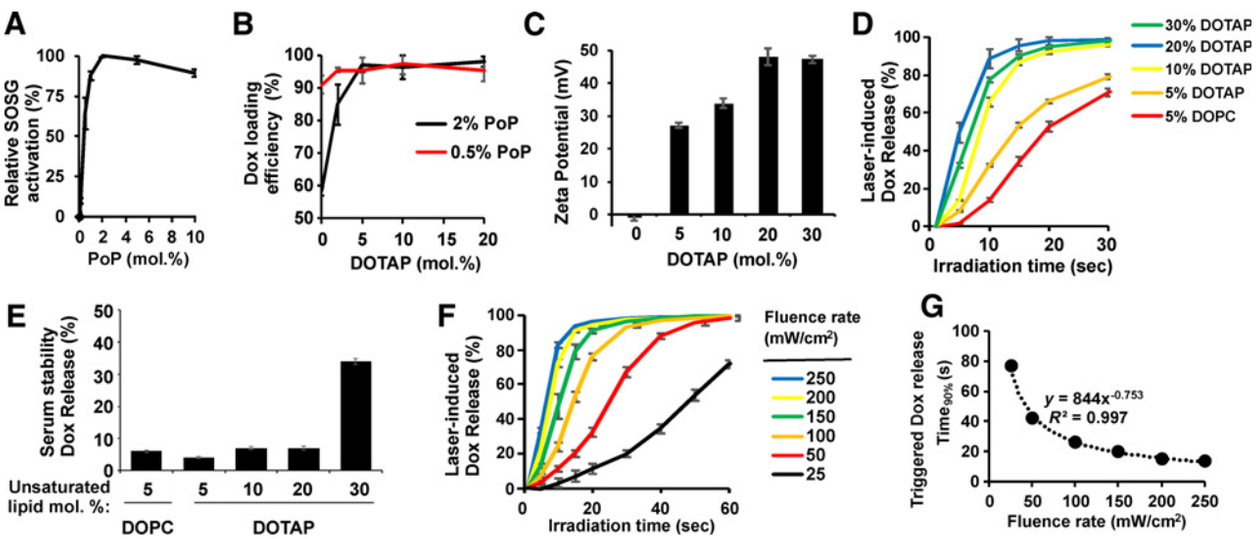

Figure 2.

Characterization of cationic DOTAP/PoP liposomes. **A,** Singlet oxygen generation (indicated by singlet oxygen green sensor SOSG after irradiation (10 s) for various PoP liposomes containing 10 mol% DOTAP. **B,** Dox loading efficiency of PoP liposomes containing various amounts of DOTAP. **C,** Zeta potential of liposomes containing 5, 10, 20, and 30 mol% DOTAP or 5 mol% DOPC. All formulations contain 2 mol% PoP. **D,** Light-triggered release (250 mW/cm^2) of Dox from liposomes. Light-triggered release was performed in 50% adult bovine serum at 37°C. **E,** Serum stability of cationic PoP liposomes (2 mol% PoP) incubated in 50% adult bovine serum at 37°C for 1 hour. **F,** Light-triggered Dox release rate of DOTAP/PoP liposomes (2 mol% PoP and 20 mol% DOTAP) at different fluence rates, performed in 50% adult bovine serum at 37°C. **G,** Time required to reach 90% light-induced release of Dox from DOTAP/PoP liposomes. Mean ± SD for $n = 3$.

Table 1. Properties of PoP liposomes used in this study

Formulation	Dox loading (%)	Zeta potential (mV)	Size (nm)	Polydispersity (PDI)	Light release of Dox $T_{50\%}$ (second)	Light release of Dox $T_{90\%}$ (second)	% Dox release in serum (1 hour)
Neutral	95 ± 3	−0.9 ± 0.9	101 ±2	0.02 ± 0.02	19 ± 0.6	76 ± 9	6 ± 0.4
5% DOTAP	98 ± 2	27.1 ± 0.8	111 ±7	0.05 ± 0.01	13 ± 2.3	40 ± 12	4 ± 0.3
10% DOTAP	96 ± 4	33.9 ± 1.4	101 ±1	0.08 ± 0.01	9 ± 0.6	17 ± 1	7 ± 0.4
20% DOTAP	98 ± 2	47.9 ± 2.3	109 ± 10	0.06 ± 0.03	5 ± 0.6	11 ± 3	7 ± 0.6
30% DOTAP	99 ± 2	47.3 ± 1.2	99 ± 3	0.07 ± 0.02	7 ± 0.0	15 ± 1	34 ± 0.9

Data show mean ± standard deviation for 3 separate measurements.
Light triggered release were performed at 250 mW/cm^2 in 50% bovine serum at 37°C. Serum stability were performed in 50% bovine serum at 37°C. Mean ± SD for $n = 3$.

DOTAP and appears to reach a maximal value at 20 mol% DOTAP. Liposomes lacking DOTAP (containing 5 mol% DOPC) were nearly neutral at −0.9 mV. The NIR light-induced release rate of these formulations was all relatively rapid, with formulations containing 20–30 mol% DOTAP completing 90% Dox release in ~15 seconds (Fig. 2D). PoP liposomes with 5–20 mol% DOTAP were stable in 50% serum, with less than 10% leakage in 1 hours. This timeframe was selected because the liposomes are short circulating and phototreated soon after injection. However, at 30 mol% DOTAP, Dox leakage increased to 30%. Thus, 20 mol.% DOTAP was selected for further study (Fig. 2E). Table 1 lists other parameters of the liposomes. The size of these formulations was close to 100 nm and the Dox loading efficiencies were all above 95%.

The light-triggered Dox release of the selected formulation with 2 mol.% PoP and 20 mol.% DOTAP at different fluence rates was studied (Fig. 2F). Increased fluence resulted increased Dox release rates. At a fluence rate of 100 mW/cm^2, over 90% Dox release occurred in 30 seconds while at 25 mW/cm^2, 80 seconds was required. The relationship between the time required to reach 90% Dox release and fluence rate fit well with a power function (Fig. 2G). Low amounts of NIR energy were required to reach 90% Dox release with this formulation, with 3.4 J/cm^2 at 250 mW/cm^2 and 2.6 J/cm^2 at 100 mW/cm^2 (Supplementary Fig. S3). When calculating the energy required for 90% Dox release at different fluence rate, a linear relationship was observed, indicating that less energy is required when lower fluence rates are applied. We previously have observed that the amount of energy to release the drug depends on the fluence rate applied (42).

Cationic PoP liposomes bind to cancer cells and vascular endothelial cells *in vitro*

Dox-loaded cationic PoP liposomes were briefly incubated with the human MIA PaCa-2 pancreatic cell line for 20 minutes and removed prior to live cell imaging with confocal fluorescence microscopy. Both Dox and PoP could independently be observed as they are both fluorescent molecules and spectrally separated. Hoechst 33342 was used to stain the nucleus. As shown in Fig. 3A, PoP liposomes with 20% DOTAP bound substantially more avidly to cells than liposomes containing 5% DOTAP. Notably,

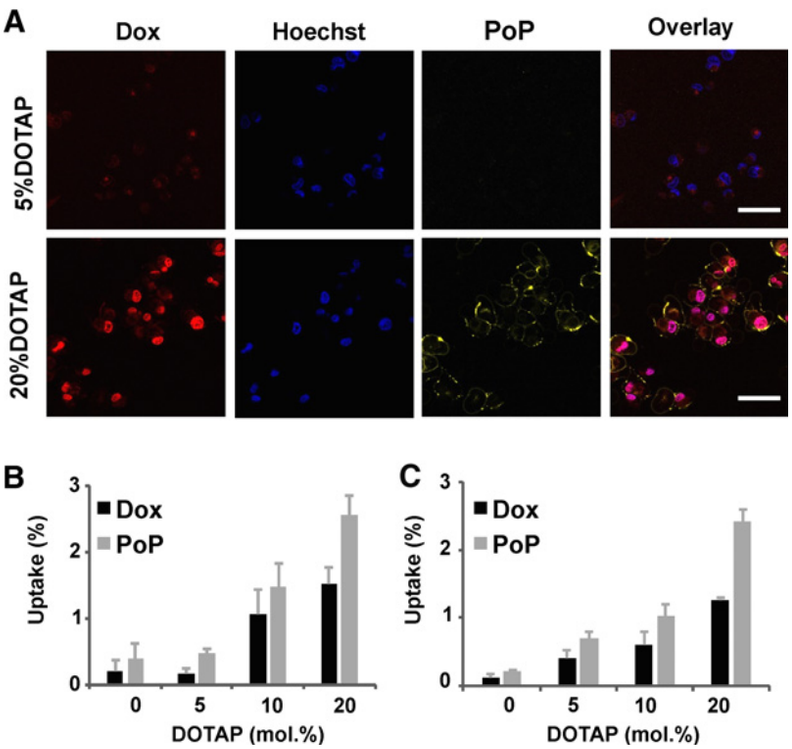

Figure 3.
Cationic PoP liposomes bind to MIA PaCa-2 cells and HUCECs *in vitro*. **A,** Dox, PoP, and overlay channels of MIA PaCa-2 cells pretreated with 10 μg/mL liposomal Dox for 20 minutes. Scale bar, 50 μm. Dox and PoP uptake in MIA PaCa-2 cells (**B**) or human vascular endothelial cells (**C**). Cells were incubated with indicated liposomes (10 μg/mL Dox) for 20 minutes, washed, then lysed with detergent for determining uptake. Data are presented as the percentage of drug accumulated in the cells as a percentage of the total amount of drug in the incubation medium. Mean ± SD for $n = 4$.

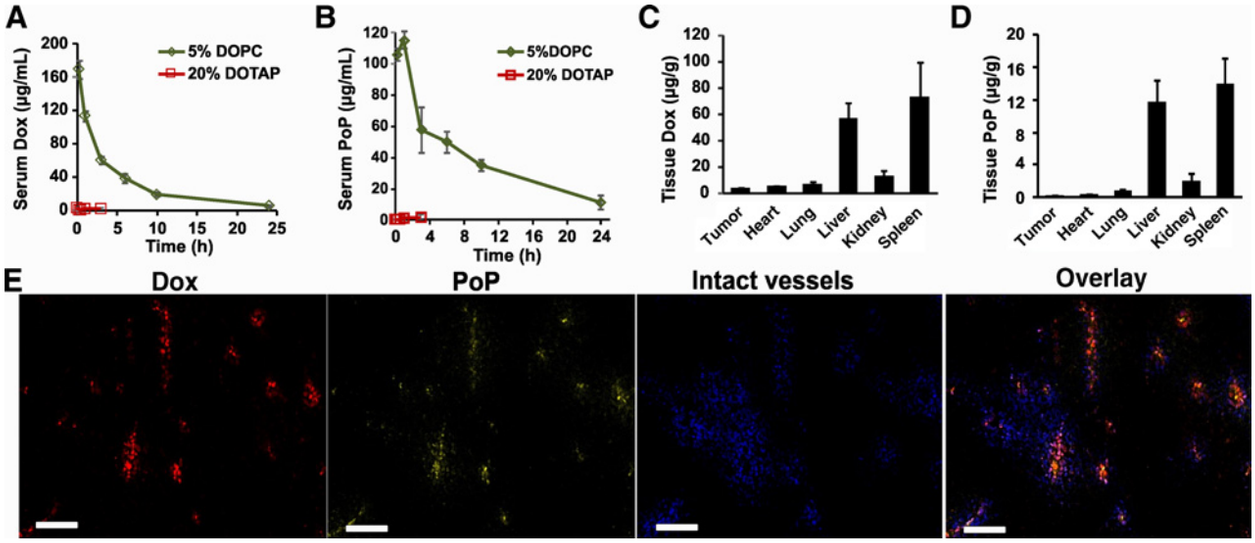

Figure 4.

Distribution of cationic PoP liposomes. **A,** Dox blood circulation of 10 mg/kg Dox encapsulated in PoP liposomes containing 5% DOPC or 20% DOTAP. Liposomes were intravenously administered in BALB/c mice ($n = 5$). **B,** PoP blood concentration after intravenous administration of 10 mg/kg Dox encapsulated in PoP liposomes containing 5% DOPC or 20% DOTAP. **C,** Biodistribution of Dox 24 hours after intravenous injection of 5 mg/kg DOTAP/PoP liposomes in MIA PaCa-2 tumor–bearing nude mice. **D,** Biodistribution of PoP 24 hours after intravenous injection of 5 mg/kg DOTAP/PoP liposomes in MIA PaCa-2 tumor–bearing nude mice. **E,** MIA PaCa-2 tumor slice fluorescence imaging from mice treated with 20% DOTAP/PoP liposomes (10 mg/kg Dox). 20 mg/kg Hoechst 33342 was intravenously injected prior to mouse sacrifice to visualize functional tumor vessels. Scale bar, 100 μm.

Dox was visualized mostly in the nucleus, demonstrating its bioavailability upon uptake. PoP exhibited a different localization pattern, with some punctate expression inside the cell, and much of the signal localized to the cell membrane. To better quantify uptake, cells were lysed following incubation and uptaken Dox and PoP was quantified relative to the total amount in the incubation (Fig. 3B). Increasing cationic character resulted in greater uptake of the liposomes with respect to both Dox and PoP. PoP apparently had higher uptake than Dox, for reasons that are not clear, but perhaps the detergent lysis extraction method was not effective at removing Dox from lysed nuclei. PoP liposomes containing 20% DOTAP had a 6.5-fold more Dox uptake and 7.9-fold more PoP uptake compared with neutral liposomes (which contained 5 mol.% DOPC). As shown in Fig. 3C, a similar trend was observed with human vascular endothelial cells (HUVEC). Compared with neutral liposomes, liposomes containing 20% DOTAP delivered 10.5-fold more Dox signal and 11.6-fold more PoP. DOTAP liposomes (20 mol. %) exhibited markedly higher uptake relative to 5 mol% DOTAP liposomes, even though both had positive zeta potentials (Table 1). Perhaps in biological conditions, higher DOTAP concentrations are required to maintain cationic character. Thus, strongly cationic PoP liposomes bind both human endothelial and pancreatic cancer cells with high avidity, likely based on charge interaction.

Accumulation of cationic PoP liposomes in tumor vasculature

The *in vivo* behavior of Dox-loaded cationic PoP liposomes (2 mol.% PoP, 20 mol.% DOTAP) was examined. Fifteen minutes following intravenous administration of 10 mg/kg Dox in cationic PoP liposomes, the amount of Dox in circulation was less than 1 μg/mL. In contrast, 168 μg/mL Dox was in blood circulation with neutral but otherwise similar PoP liposomes (2 mol% PoP, 5 mol% DOPC; Fig. 4A). Both liposomes were stable in serum in this time period (Table 1; Fig. 2E), so the difference was not due to liposome instability. Similar to Dox, cationic PoP liposomes themselves were rapidly cleared from circulation, with negligible PoP signal identified 15 minutes post administration (Fig. 4B). This striking difference is consistent with literature results demonstrating that cationic liposomes are cleared very rapidly from the blood stream, with less than a 5-minute half-life (44). Pharmacokinetic behavior of the cationic liposomes could not be analyzed due to this rapid clearance, but Table S1 shows the pharmacokinetics parameters of the neutral Dox PoP liposomes by noncompartmental analysis. The biodistribution of the cationic PoP liposomes following intravenous injection was next examined in tumor-bearing mice. The majority of DOTAP/PoP liposomes accumulated in the liver and spleen (Fig. 4C; Supplementary Fig. S4). The rapid clearance of cationic liposomes results predominantly from rapid uptake by macrophages of the reticular endothelial system in the liver and spleen (44). However, some Dox (3 μg/kg) was detected in the tumor. A similar distribution pattern was found with PoP itself (Fig. 4D). To further study the spatial distribution of cationic PoP liposomes in tumor, fluorescence microscopy of tumor slices was performed. Hoechst 33342 (20 mg/kg) was intravenously injected immediately prior to mouse sacrifice in order to locate functional tumor vessels, as has previously been reported (45). As shown in Fig. 4E, the PoP and Dox signals overlapped with intact vessels and were restricted to nearby the endothelial cells, but not in the tumor space. This is in accordance with literature suggesting that cationic liposomes preferentially bind to the tumor vasculature with minimal extravasation into the tumor interstitium (44, 46). An example of a smaller region of the tumor slice shown in Supplementary Fig. S5 also demonstrated that Dox and PoP were colocalized with Hoechst near the tumor vessels.

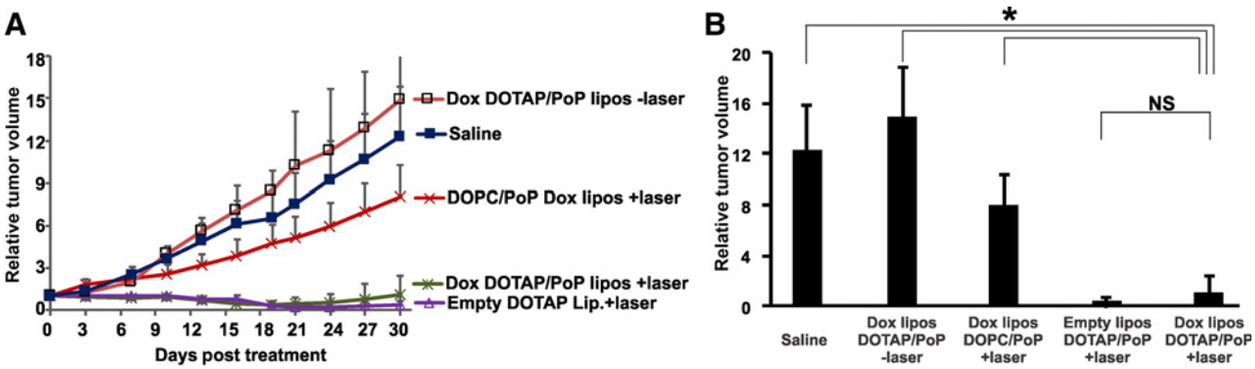

Figure 5.

Treatment conditions resulting in dominant vascular PDT with cationic PoP liposomes. **A,** Relative tumor volumes of mice intravenously administered 5 mg/kg liposomal Dox or equivalent. Initial tumor volumes were 70–120 mm^3 (5–8 mm in length). 665 nm laser diode treatment was initiated 15 minutes post administration at 200 mW/cm^2 for 8.3 minutes (100 J/cm^2). **B,** Relative tumor volumes at day 30. The asteroid indicates significance (*, $P < 0.05$, Mann–Whitney *t* test); "NS", not significant. Mean ± SD for $n = 5$–6 mice per group.

Vascular targeted PDT effect by cationic PoP liposomes

The antitumor efficacy of Dox-loaded, cationic PoP liposomes was evaluated in mice bearing subcutaneous MIA PaCa-2 xenografts. Fifteen minutes following administration, mice were treated with a 665-nm laser diode at 200 mW/cm^2 for 8.3 minutes (100 J/cm^2). As shown in Fig. 5A, 5 mg/kg Dox-loaded DOTAP/PoP liposomes alone were ineffective in preventing tumor growth. Dox-loaded DOPC liposomes (5 mg/kg) with laser treatment also did not significantly inhibit the tumor growth ($P = 0.095$, DOPC liposomes + laser compared with saline). However, Dox-loaded DOTAP/PoP liposomes with laser treatment significantly inhibited tumor growth ($P = 0.016$, DOTAP/PoP liposomes + laser compared with saline), resulting in a 91% tumor reduction and 25% cure rate. Dox-loaded DOTAP/PoP liposomes with phototreatment were significantly more effective than Dox-loaded DOPC/PoP liposomes with phototreatment ($P = 0.016$), suggesting that cationic PoP liposomes have stronger vascular PDT effect (Fig. 5B). This enhanced PDT effect is likely due to the accumulation of DOTAP/PoP liposomes within the vessels. Unexpectedly, unloaded DOTAP/PoP liposomes with laser treatment demonstrated similar efficacy as loaded DOTAP/PoP liposomes with the same laser treatment ($P = 0.29$). The laser-treated site of the mice swelled 1 to 3 hours post laser treatment and an eschar formed 2 to 3 days after laser treatment. Supplementary Fig. S6 shows that scars form on the tumors of the mice treated with DOTAP/PoP liposomes and empty DOTAP/PoP liposomes, but not the DOPC/PoP liposomes + laser group. Mice treated with Dox-loaded DOTAP/PoP liposomes+laser or empty DOTAP/PoP liposomes+laser at this dose exhibited minor signs of toxicity during the first 3 days after treatment with a ~6% body weight loss in both groups (Supplementary Fig. S7).

Synergistic chemo- and phototherapeutic effects

Chemophototherapy combines both chemo- and phototherapeutic modalities. Interestingly, in the conditions initially examined in Fig. 5, the chemotherapeutic component did not contribute and PDT alone exerted dominant effects for tumor shrinkage (based on efficacy of unloaded cationic liposomes). We next attempted to modulate conditions so that synergistic effects could be observed. Given the strong PDT effect at the previous laser treatment condition (200 mW/cm^2 for 8.3 minutes, 100 J/cm^2), the laser dose was reduced to 100 mW/cm^2 for 3.3 minutes (20 J/cm^2), or just 20% of the previous total laser dose. Because ablation efficacy depends on both the light dose and the drug dose, it may be possible that the physiological relevance of using lower light doses would be expected to occur at locations deep in the irradiated tumor. In other words, there would be partial volumes deep in a treated tumor that receive this light dose. As shown in Fig. 6A and B, Dox-loaded DOTAP/PoP liposomes at 7 mg/kg without phototreatment were not effective against MIA PaCa-2 tumors, as the tumor volumes were not significantly different from that of saline group at day 31 ($P = 0.29$). Empty DOTAP/PoP liposomes with laser treatment were able to significantly reduce the tumor growth by 57.2% at day 31 (empty DOTAP/PoP liposomes vs. saline, $P = 0.016$). Following tumor treatment with Dox-loaded DOTAP/PoP liposomes and laser, the growth of the tumors was significantly retarded compared with saline group, leading to 85.2% of tumor growth inhibition and a 25% cure rate at day 31 (DOTAP/PoP liposomes vs. saline, $P = 0.008 < 0.01$). Empty DOTAP/PoP liposomes were not as effective as the drug-loaded DOTAP/PoP liposomes as tumor volumes in empty DOTAP/PoP liposomes+laser group were significantly higher than loaded DOTAP/PoP liposomes+laser at day 31 (*, $P = 0.032 < 0.05$, Mann–Whitney test). When looking at the days for the tumors to double its initial tumor volume, Dox-loaded DOTAP/PoP liposomes without laser treatment was able to delay the tumor growth by just 3.2 days (DOTAP/PoP liposomes-laser vs. saline, 9.8 days vs. 6.6 days), indicating that Dox-loaded DOTAP/PoP liposomes have only minor efficacy in inhibiting the tumor growth initially. With laser treatment, both Dox-loaded DOTAP/PoP liposomes and empty DOTAP/PoP liposomes demonstrated a significantly longer time to reach twice of the initial tumor volume. Dox-loaded DOTAP/PoP liposomes + laser significantly delayed the time for tumors to reach twice the initial volume compared with empty DOTAP/PoP liposomes + laser (30.2 days vs. 16.2 days; *, $P = 0.026$, Fig. 6C), with 40% of tumors cured at day 46 in the Dox-loaded DOTAP/PoP + laser group and 0% cure rate from empty DOTAP/PoP liposomes + laser group. The combined tumor growth delay for [Dox-loaded DOTAP/POP liposomes − laser] combined with [empty PoP liposomes + laser] was 19.4 days, whereas [DOTAP Dox liposomes + laser] delayed the tumor growth by 30.2 days, suggesting

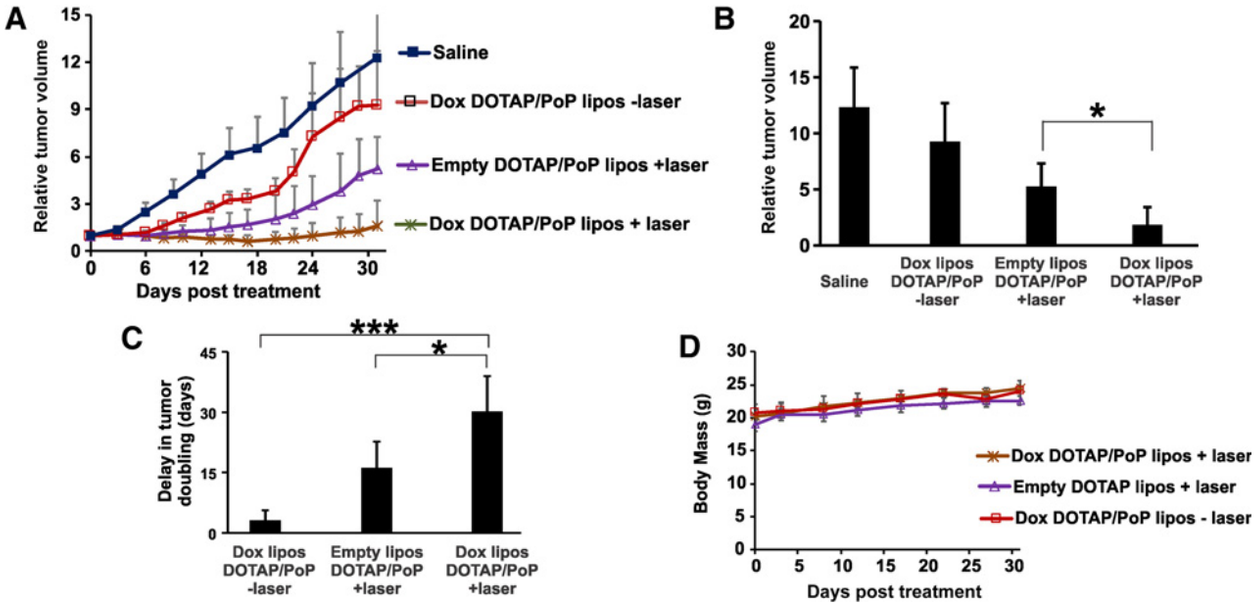

Figure 6.

Conditions for synergistic chemophototherapy. **A,** Relative tumor volumes of mice administered DOTAP PoP liposomes (7 mg/kg Dox) or equivalent. Short laser treatment (100 mW/cm^2 for 3.3 minutes, 20 J/cm^2) was initiated 15 minutes post injection. Initial tumor volumes were 70–120 mm^3 (5–8 mm in length). **B,** Relative tumor volumes of mice from each groups at day 31 post treatment. The asterisk indicates significant differences (*, $P < 0.05$; **, $P < 0.01$, Mann–Whitney t test). **C,** Delay for tumor to double its initial tumor volume. Asterisks indicate significance differences (*, $P < 0.05$; ***, $P < 0.001$, Mann–Whitney t test). **D,** Body mass of treated mice. $N = 5$–6 mice per group.

that vascular targeted chemo- and photo therapeutic effects were synergistic in delaying tumor growth. The mice tolerated this treatment well and no weight loss occurred (Fig. 6D).

Tumor blood flow during laser treatment

Laser Doppler imaging was used to monitor the tumoral blood flow during the treatment course. Following administration of 7 mg/kg Dox in the conditions that chemophototherapy was synergistic, the blood flow in the tumor was stabilized before laser treatment. As shown in Fig. 7, after the laser was applied, the blood flow in the tumor immediately dropped to ~30% of the original blood flow. However, the blood flow recovered gradually after the laser was off. The temporal vascular effects were likely the characteristic of vasoconstriction, rather than thrombus formation (47).

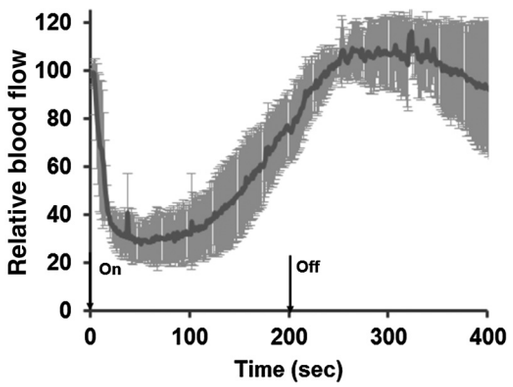

Figure 7.

Tumor blood flow during vessel-targeted chemophototherapy. Relative tumor blood flow during the laser treatment assessed in real time by laser Doppler measurement following intravenous administration of 7 mg/kg Dox in DOTAP/PoP liposomes. The arrows indicate the initiation and end of laser treatment. Mean ± SD for $n = 3$.

Discussion

Cationic liposomes were first introduced in gene delivery as an alternative to viral vectors, with many cationic liposomes tested in clinical trials for gene therapy (48). However, the clinical outcomes of cationic liposomes for gene delivery is far from satisfactory due to the low transfection efficiency *in vivo* (48, 49). Dose-dependent toxicity could also be an obstacle of the application of cationic liposomes (50). More recently, the preferential accumulation of cationic liposomes in tumor endothelial cells has been observed (13, 15, 51). EndoTAG-1 is a cationic DOTAP preparation of paclitaxel that has completed phase II clinical trials in HER2-negative breast cancer (NCT00448305 and NCT01537536), pancreatic cancer (NCT00377936), and liver cancer (NCT00542048). Enhancement of therapeutic efficacy has been observed compared with conventional chemotherapy in lung and pancreatic cancers (52). EndoTAG-2, a cationic liposomal formulation of camptothecin, has also shown improved antitumor efficacy by tumor vascular targeting (46). Thus, DOTAP formulations do have potential for clinical translation.

We previously found that unsaturated lipids (e.g., DOPC) accelerate NIR light-triggered release of Dox from PoP liposomes (42). When DOTAP, an unsaturated cationic lipid, was incorporated into PoP liposomes, the release rate of encapsulated Dox was

extremely rapid, with complete light-triggered Dox release occurring in just 15 seconds. The mechanism of accelerated light activated drug release is likely due to oxidation of the unsaturated lipid DOTAP via reactive oxygen species generated upon light irradiation. Interestingly, DOTAP had an effect of improving Dox loading into PoP liposomes, especially when PoP amounts were over 0.5 mol. %. However, high amount of DOTAP (over 30 mol. %) resulted in Dox leakage during serum incubation.

Cationic PoP liposomes bound to cancer cells such as MIA PaCa-2 and vascular endothelial cells HUVECs *in vitro*. A 8- to 12-fold increase of liposomes accumulation was seen with DOTAP/PoP liposomes compared with DOPC/PoP liposomes. This is in accordance with results from Thurston and colleagues that showed that angiogenic endothelial cells have an average of 15- to 33-fold more uptake of cationic liposomes (DOTAP/cholesterol) than corresponding normal endothelial cells (15).

Cationic PoP liposomes were rapidly cleared from blood circulation, and some cationic PoP liposomes were detected in the tumor vasculature (Fig. 4D). This is likely due to rapid uptake by the macrophages in liver and spleen (44, 53). Using the cationic liposomal vesicles, Dolmans and colleagues demonstrated that the vascular accumulation of photosensitizers determines the tumor response (47). Although the overall amount of PoP in the tumor was low, the majority of PoP was presumably attached to the endothelial cells. As a result, NIR irradiation induced a remarkably potent vascular PDT effect. With a relatively short light treatment of 8.3 minutes (200 mW/cm^2 and 100 J/cm^2), Dox-loaded DOTAP PoP liposomes were significantly more effective than neutral ones due to the much stronger PDT effect in the DOTAP/PoP liposomes group. However, empty liposomes had an equally potent effect, demonstrating that the observed antitumor effects were dominated by PDT.

To find synergy, the light dose reduced to just 20% of the previous light dose (from 100 to 20 J/cm^2) and the drug dose was increased from 5 mg/kg to 7 mg/kg. In this case, vascular PDT alone had some efficacy in inhibiting the tumor growth, whereas Dox-loaded PoP liposomes alone without laser treatment were ineffective. However, drug-loaded DOTAP/PoP liposomes with laser treatment were significantly more effective than either chemo- or phototherapy alone, indicating a synergistic effect of PDT and chemotherapy of this single-agent treatment approach. The significance of using an extremely low light dose can be justified because in a clinical scenario of treating a large tumor, as light is rapidly attenuated in tissue, deeper tissues will receive less light.

In conclusion, we developed cationic PoP liposomes that rapidly release an encapsulated anticancer drug upon NIR irradiation and that bind to both tumor and vascular endothelial cells *in vitro*. Following intravenous administration, Dox-loaded cationic PoP liposomes accumulated in tumor vessels, leading to potent vascular PDT effects upon irradiation at low laser power and, depending on the treatment conditions, synergistic chemophototherapy effects for tumor growth inhibition.

Disclosure of Potential Conflicts of Interest

No potential conflicts of interest were disclosed.

Authors' Contributions

Conception and design: D. Luo, J.F. Lovell
Development of methodology: D. Luo, J. Geng, S. Shao
Acquisition of data (provided animals, acquired and managed patients, provided facilities, etc.): D. Luo, J. Geng, K.A. Carter
Analysis and interpretation of data (e.g., statistical analysis, biostatistics, computational analysis): D. Luo, J. Geng, K.A. Carter
Writing, review, and/or revision of the manuscript: D. Luo, J.F. Lovell
Administrative, technical, or material support (i.e., reporting or organizing data, constructing databases): J. Geng
Study supervision: J.F. Lovell
Other (designed and conducted LC-MS experiment; analyzed LC-MS data): N. Li
Other (supervised the acquisition and analysis of LC-MS experiments): G.E. Atilla-Gokcumen

Acknowledgments

The authors thank Dr. Ruogang Zhao for assistance with cell studies and Alan Siegel (SUNY, University at Buffalo) for help with confocal microscopy.

Grant Support

This work was supported by the NIH (R01EB017270 and DP5OD017898) and the National Science Foundation (1555220).

The costs of publication of this article were defrayed in part by the payment of page charges. This article must therefore be hereby marked *advertisement* in accordance with 18 U.S.C. Section 1734 solely to indicate this fact.

Received April 4, 2017; revised June 2, 2017; accepted July 5, 2017; published OnlineFirst July 20, 2017.

References

1. Folkman J. Role of angiogenesis in tumor growth and metastasis. Semin Oncol 2002;29(6, Supplement 16):15–8.
2. Liotta LA, Steeg PS, Stetler-Stevenson WG. Cancer metastasis and angiogenesis: an imbalance of positive and negative regulation. Cell 1991;64:327–36.
3. Zetter BR. Angiogenesis and tumor metastasis. Annu Rev Med 1998;49:407–24.
4. Carmeliet P, Jain RK. Angiogenesis in cancer and other diseases. Nature 2000;407:249–57.
5. Neri D, Bicknell R. Tumour vascular targeting. Nat Rev Cancer 2005;5:436–46.
6. Heldin C, Rubin K, Pietras K, Ostman A. High interstitial fluid pressure-an obstacle in cancer therapy. Nat Rev Cancer 2004;4:806.
7. Niu G, Chen X. Why integrin as a primary target for imaging and therapy. Theranostics 2011;1:30–47.
8. Ellis LM, Hicklin DJ. VEGF-targeted therapy: mechanisms of anti-tumour activity. Nat Rev Cancer 2008;8:579–91.
9. Fonsatti E, Altomonte M, Nicotra MR, Natali PG, Maio M. Endoglin (CD105): a powerful therapeutic target on tumor-associated angiogenetic blood vessels. Oncogene 0000;22:6557–63.
10. Arap W, Pasqualini R, Ruoslahti E. Cancer treatment by targeted drug delivery to tumor vasculature in a mouse model. Science 1998;279:377–80.
11. Murphy EA, Majeti BK, Barnes LA, Makale M, Weis SM, Lutu-Fuga K, et al. Nanoparticle-mediated drug delivery to tumor vasculature suppresses metastasis. Proc Natl Acad Sci 2008;105:9343–8.
12. Zhen Z, Tang W, Chuang Y-J, Todd T, Zhang W, Lin X, et al. Tumor vasculature targeted photodynamic therapy for enhanced delivery of nanoparticles. ACS Nano 2014;8:6004–13.
13. Abu LA, Ishida T, Kiwada H. Targeting anticancer drugs to tumor vasculature using cationic liposomes. Pharm Res 2010;27:1171.
14. Campbell R, Ying B, Kuesters G, Hemphill R. Fighting cancer: from the bench to bedside using second generation cationic liposomal therapeutics. J Pharm Sci 2009;98:411.

15. Thurston G, McLean JW, Rizen M, Baluk P, Haskell A, Murphy TJ, et al. Cationic liposomes target angiogenic endothelial cells in tumors and chronic inflammation in mice. J Clin Invest 1998;101:1401.
16. Wu J, Lee A, Lu Y, Lee RJ. Vascular targeting of doxorubicin using cationic liposomes. Int J Pharm 2007;337:329–35.
17. Pastorino F, Brignole C, Marimpietri D, Cilli M, Gambini C, Ribatti D, et al. Vascular damage and anti-angiogenic effects of tumor vessel-targeted liposomal chemotherapy. Cancer Res 2003;63:7400–09.
18. Abu Lila AS, Kizuki S, Doi Y, Suzuki T, Ishida T, Kiwada H. Oxaliplatin encapsulated in PEG-coated cationic liposomes induces significant tumor growth suppression via a dual-targeting approach in a murine solid tumor model. J Control Release 2009;137: 8–14.
19. Krasnici S, Werner A, Eichhorn ME, SchmittSody M, Pahernik SA, Sauer B, et al. Effect of the surface charge of liposomes on their uptake by angiogenic tumor vessels. Int J Cancer 2003;105:561–67.
20. Ran S, Downes A, Thorpe P. Increased exposure of anionic phospholipids on the surface of tumor blood vessels. Cancer Res 2002;62:6132.
21. Lohr JM, Haas SL, Bechstein WO, Bodoky G, Cwiertka K, Fischbach W, et al. Cationic liposomal paclitaxel plus gemcitabine or gemcitabine alone in patients with advanced pancreatic cancer: a randomized controlled phase II trial. Ann Oncol 2012;23:1214–22.
22. Dougherty TJ, Gomer CJ, Henderson BW, Jori G, Kessel D, Korbelik M, et al. Photodynamic therapy. J Natl Cancer Inst 1998;90:889–905.
23. Agostinis P, Berg K, Cengel KA, Foster TH, Girotti AW, Gollnick SO, et al. Photodynamic therapy of cancer: an update. CA Cancer J Clin 2011;61: 250–81.
24. Sato K, Hanaoka H, Watanabe R, Nakajima T, Choyke PL, Kobayashi H. Near infrared photoimmunotherapy in the treatment of disseminated peritoneal ovarian cancer. Mol Cancer Ther 2015;14:141–50.
25. Wang X, Tsui B, Ramamurthy G, Zhang P, Meyers J, Kenney ME, et al. Theranostic agents for photodynamic therapy of prostate cancer by targeting prostate-specific membrane antigen. Mol Cancer Ther 2016;15: 1834–44.
26. Zuluaga M-F, Sekkat N, Gabriel D, van den Bergh H, Lange N. Selective photodetection and photodynamic therapy for prostate cancer through targeting of proteolytic activity. Mol Cancer Ther 2013;12:306–13.
27. Chen B, Pogue BW, Hoopes PJ, Hasan T. Combining vascular and cellular targeting regimens enhances the efficacy of photodynamic therapy. Int J Radiat Oncol Biol Phys 2005;61:1216–26.
28. Trachtenberg J, Bogaards A, Weersink RA, Haider MA, Evans A, McCluskey SA, et al. Vascular targeted photodynamic therapy with palladium-bacteriopheophorbide photosensitizer for recurrent prostate cancer following definitive radiation therapy: assessment of safety and treatment response. J Urol 2007;178:1974–9.
29. Reddy GR, Bhojani MS, McConville P, Moody J, Moffat BA, Hall DE, et al. Vascular targeted nanoparticles for imaging and treatment of brain tumors. Clin Cancer Res 2006;12:6677–86.
30. Zhou A, Wei Y, Wu B, Chen Q, Xing D. Pyropheophorbide A and c (RGDyK) comodified chitosan-wrapped upconversion nanoparticle for targeted near-infrared photodynamic therapy. Mol Pharm 2012;9: 1580–9.
31. Cheng S-H, Lee C-H, Chen M-C, Souris JS, Tseng F-G, Yang C-S, et al. Trifunctionalization of mesoporous silica nanoparticles for comprehensive cancer theranostics-the trio of imaging, targeting and therapy. J Mater Chem 2010;20:6149–57.
32. Carter KA, Shao S, Hoopes MI, Luo D, Ahsan B, Grigoryants VM, et al. Porphyrin-phospholipid liposomes permeabilized by near-infrared light. Nat Commun 2014;5:3546.
33. Luo D, Carter K, Razi A, Geng J, Shao S, Lin C, et al. Porphyrin-phospholipid liposomes with tunable leakiness. J Control Release 2015;220(Pt A):484.
34. Luo D, Carter K, Razi A, Geng J, Shao S, Giraldo D, et al. Doxorubicin encapsulated in stealth liposomes conferred with light-triggered drug release. Biomaterials 2016;75:193.
35. Carter KA, Luo D, Razi A, Geng J, Shao S, Ortega J, et al. Sphingomyelin liposomes containing porphyrin-phospholipid for irinotecan chemophototherapy. Theranostics 2016;6:2329–36.
36. Carter K, Wang S, Geng J, Luo D, Shao S, Lovell J. Metal chelation modulates phototherapeutic properties of mitoxantrone-loaded porphyrin-phospholipid liposomes. Mol Pharm 2016;13:420.
37. Huang H, Mallidi S, Liu J, Chiang C, Mai Z, Goldschmidt R, et al. Photodynamic therapy synergizes with irinotecan to overcome compensatory mechanisms and improve treatment outcomes in pancreatic cancer. Cancer Res 2016;76:1066.
38. Zuluaga M, Lange N. Combination of photodynamic therapy with anticancer agents. Curr Med Chem 2008;15:1655.
39. Luo D, Carter KA, Miranda D, Lovell JF. Chemophototherapy: an emerging treatment option for solid tumors. Adv Sci 2016. DOI: 10.1002/advs.201600106.
40. Spring BQ, Bryan Sears R, Zheng LZ, Mai Z, Watanabe R, Sherwood ME, et al. A photoactivable multi-inhibitor nanoliposome for tumour control and simultaneous inhibition of treatment escape pathways. Nat Nano 2016;11:378–87.
41. Rwei AY, Wang W, Kohane DS. Photoresponsive nanoparticles for drug delivery. Nano Today 2015;10:451–67.
42. Luo D, Li N, Carter K, Lin C, Geng J, Shao S, et al. Rapid light-triggered drug release in liposomes containing small amounts of unsaturated and porphyrin-phospholipids. Small 2016;12:3039.
43. Haran G, Cohen R, Bar LK, Barenholz Y. Transmembrane ammonium sulfate gradients in liposomes produce efficient and stable entrapment of amphipathic weak bases. Biochim Biophys Acta 1993;1151:201–15.
44. McLean J, Fox E, Baluk P, Bolton P, Haskell A, Pearlman R, et al. Organ-specific endothelial cell uptake of cationic liposome-DNA complexes in mice. Am J Physiol 1997;273:H387.
45. Roy Chaudhuri T, Straubinger NL, Pitoniak RF, Hylander BL, Repasky EA, Ma WW, et al. Tumor-priming smoothened inhibitor enhances deposition and efficacy of cytotoxic nanoparticles in a pancreatic cancer model. Mol Cancer Ther 2016;15:84–93.
46. Eichhorn M, Luedemann S, Strieth S, Papyan A, Ruhstorfer H, Haas H, et al. Cationic lipid complexed camptothecin (EndoTAG-2) improves antitumoral efficacy by tumor vascular targeting. Cancer Biol Ther 2007;6:920.
47. Dolmans D, Kadambi A, Hill J, Waters C, Robinson B, Walker J, et al. Vascular accumulation of a novel photosensitizer, MV6401, causes selective thrombosis in tumor vessels after photodynamic therapy. Cancer Res 2002;62:2151.
48. Simões S, Filipe A, Faneca H, Mano M, Penacho N, Düzgünes N, et al. Cationic liposomes for gene delivery. Expert Opin Drug Deliv 2005;2:237.
49. Audouy S, de Leij L, Hoekstra D, Molema G. In vivo characteristics of cationic liposomes as delivery vectors for gene therapy. Pharm Res 2002;19:1599.
50. Lv H, Zhang S, Wang B, Cui S, Yan J. Toxicity of cationic lipids and cationic polymers in gene delivery. J Control Release 2006;114:100.
51. Dicheva B, ten Hagen T, Li L, Schipper D, Seynhaeve A, van Rhoon G, et al. Cationic thermosensitive liposomes: a novel dual targeted heat-triggered drug delivery approach for endothelial and tumor cells. Nano Lett 2013;13: 2324.
52. Eichhorn M, Ischenko I, Luedemann S, Strieth S, Papyan A, Werner A, et al. Vascular targeting by EndoTAG-1 enhances therapeutic efficacy of conventional chemotherapy in lung and pancreatic cancer. Int J Cancer 2010;126: 1235.
53. Litzinger D, Brown J, Wala I, Kaufman S, Van G, Farrell C, et al. Fate of cationic liposomes and their complex with oligonucleotide in vivo. Biochim Biophys Acta 1996;1281:139.